Bidirectional Power sharing in an AC/DC System with a Dual Active Bridge Converter

Amit Jyoti Datta[1*], Arindam Ghosh[1], Firuz Zare[2] and Sumedha Rajakaruna[1]

[1] Electrical and Computer Engineering Department, Curtin University, Bentley, Western Australia, Australia
[*]amit.jyoti.datta@gmail.com
[2] School of ITEE, University of Queensland, St Lucia, Brisbane, Qld, Australia

Abstract: This paper introduces a bidirectional power sharing scheme between an ac electric utility and a dc microgrid. These two are connected together through an interlinking converter (IC) and a dual active bridge (DAB). The proposed control scheme allows predefined amount of power to be supplied from the ac to dc side or the other way around. The dual active bridge is connected at the dc side of the interlinking converter and it controls the bidirectional power flow. The dc microgrid contains dc-dc converters, where boost converters are used with the sources and buck converters are used to supply loads. These dc-dc converters and the DAB are controlled by state feedback with integral control in a linearized discrete domain. The DAB linearization and control law are presented in details. The dc microgrid is controlled by conventional V-P droop where the power from/to the ac side is considered as negative/positive load. Detailed simulation results are presented to validate the proposal. Also some hardware results are included that support the findings.

Key words: DC Microgrid, Voltage Source Converter, Dual Active Bridge and Power Flow Control.

1. Introduction

Microgrid is a concept where local loads are fed from the local generation and together they can operate in either grid connected or islanded modes. Microgrid has gained enormous popularity with the development of electrical power harnessing from photovoltaic, wind, fuel cells etc. Rapid advancement in the battery storage technology are also occurring to cope up with the intermittency of renewable energy based power generation.

A large majority of electrical loads, such as LED lighting, adjustable speed motors, electric vehicles, computing and communication equipment need dc supply. At the same time, many distributed energy resources (DERs) like PV, batteries, fuel cell produce power at dc voltage level, which is then converted in ac for grid connection. Moreover, there is potential to directly connect a wind turbine or microturbine to a dc grid. Increasingly a large number of researchers are proposing the use of dc grid at the distribution level as this reduces conversion losses significantly. Voltage transformation from one level to another in a dc grid can be achieved through dc-dc converters, which have around 95% efficiency [1].

To connect a dc microgrid with a utility or an ac microgrid, a voltage source converter (VSC) is required for ac/dc power conversion. It has been shown in a hybrid ac/dc microgrid, the ac microgrid with its local loads and dc microgrid with its local loads can coexist [2-4].

Power sharing in a hybrid microgrid in a controlled manner has remained a challenge with the growth of power generation from renewable sources. Rodriguez et al proposed a system with optimized use of battery storage and reduced dependency on utility grid to support the required amount of power in a hybrid microgrid [4]. In [2-3], autonomous control of hybrid microgrid is discussed based on normalizing the droop coefficients. But Qi et al [5] pointed out that large frequency variation leads to poor performance of the microgrid system in the aforementioned method. Xia et al [6] mentioned that most of the methods to date are only applicable if multiple microgrids have similar power ratings and to address this issue, a distributed coordination power control strategy is adopted. In their research, a battery storage supports the ac side voltage and the IC is designed to provide voltage support to the dc side of IC. In [7], a bidirectional switch has been used to control the power flow between the two sides of the hybrid microgrid.

In this paper, a DAB has been coupled with a VSC that has been called the interlinking converter (IC). A DAB contains two H-bridges that are connected together through a high frequency transformer. The DAB and IC combination facilitates bidirectional power flow.

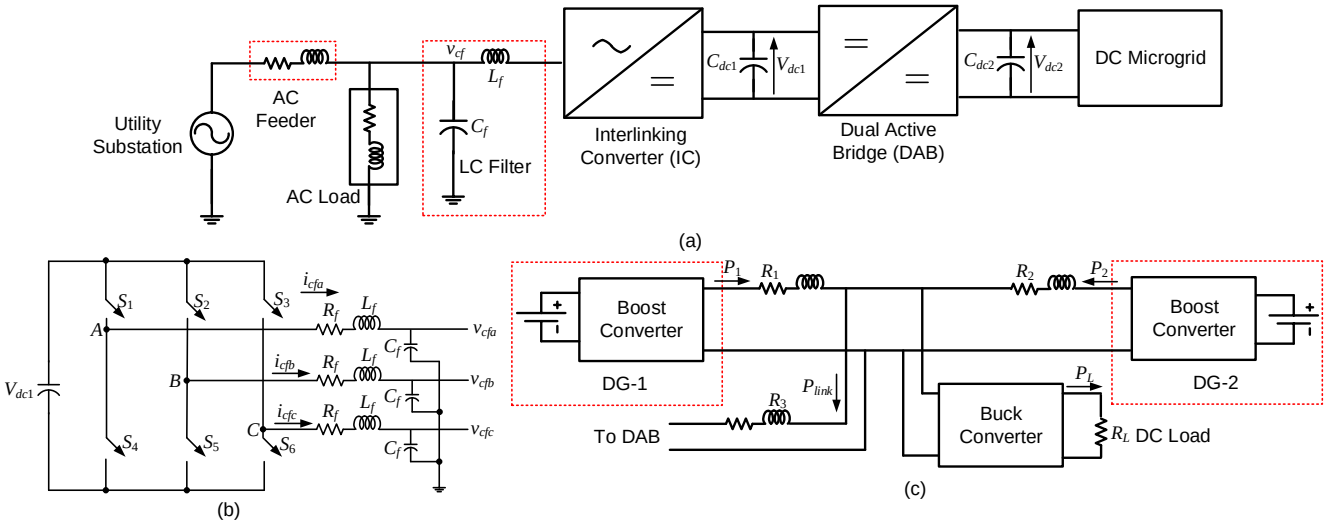

Fig. 1. *(a) The overall system structure, (b) Schematic diagram of the IC and (b) the structure of the dc microgrid.*

Power sharing in the ac microgrid is governed by the frequency droop equation, while the power sharing in the dc microgrid is designed with the voltage droop equation [2-3]. This results in a mismatch of droop coefficient if it is intended to supply power from one side to another. Subsequently power flow from ac microgrid to dc microgrid through the interlinking converter and vice versa could not be defined with a common droop equation. In view of this, the main contribution of the paper is to develop the underlying principle of operation of a dc microgrid (DCMG) that is connected with a utility system to provide a smooth bidirectional power flow. For this, a linearized model for the DAB has been developed, based on which a state feedback with integral controller is developed. Through the control method, the dc microgrid side voltage of the DAB is modulated, while its output voltage is held constant by the IC. The proposal is validated both through simulation and experimental results.

2. The System Structure

Usually DCMGs are connected with a utility system through ac/dc conversion stages [8]. Therefore the overall system structure is shown in Fig. 1 (a). The DCMG is connected to the utility system through an interlinking converter (IC) and a dual active bridge (DAB). The IC is a voltage source converter (VSC) that holds the dc voltage V_{dc1} across the capacitor C_{dc1} constant. The IC has an ac side LC filter (L_f and C_f). Given that V_{dc1} is held constant by the IC, the DAB modulates the voltage V_{dc2} across C_{dc2} to facilitate the bidirectional power flow.

When a DCMG is connected to an ac system, it is expected that the ac voltage will be high. The voltage can be brought to the level of DCMG by a transformer at the input of the IC. However, for medium voltage systems, only a VSC is sufficient. In this case the DAB transformer can provide the required isolation. In Fig. 1 (a), the IC holds the dc voltage (V_{dc1}). Therefore it cannot enable power flow control since it might adversely affect the power control in the DCMG. With the inclusion of the DAB, the separation between the voltages V_{dc1} and V_{dc2} is achieved. Now V_{dc2} can be controlled for power flow. In fact, this configuration has also been suggest in [8].

A simple DCMG structure is considered as shown in Fig. 1 (c). It contains two boost converters and a buck converter. The boost converters step up the voltage generated by the DGs to a dc distribution level, while the buck converter steps down the voltage for supplying dc loads. All these converters are controlled through their duty ratio to track the desired output voltage. The resistances R_1 and R_2 are the line resistances, while the inductors are damping inductors. The DAB is connected to the dc distribution line through a resistor R_3 and the power flow between the ac and the dc system is denoted by P_{link} with the positive direction indicated in the figure. The direction of power flow from DGs is also indicated in the figure.

The IC is a transformer-less three-phase, three-leg VSC, the schematic diagram of which is shown in Fig. 1 (b). In this figure, each switch represents an insulated gate bipolar transistor (IGBT) along with a snubber circuit and an anti-parallel diode. The dc link of the IC is connected with the DAB. An LC filter (L_f-C_f) is connected at the ac side of the IC to suppress the high frequency switching harmonics. The resistance R_f represents the converter losses. The purpose of the IC is to convert ac voltage into dc. To do this it must regulate to the voltage v_{cf} across the filter capacitor C_f (See Fig. 1) and hold the dc side voltage V_{dc1} constant. The ac voltage references are given by

$$\begin{aligned} v^*_{cfa}(t) &= V_m \sin(\omega t + \delta) \\ v^*_{cfb}(t) &= V_m \sin(\omega t + \delta - 120^\circ) \\ v^*_{cfc}(t) &= V_m \sin(\omega t + \delta + 120^\circ) \end{aligned} \qquad (1)$$

where V_m is a pre-specified voltage magnitude, ω is frequency of the system in rad/s and δ is obtained from the power balance in the ac side as discussed below.

In any VSC, the dc link voltage should roughly be around 1.5 times the line-to-line ac voltage to be synthesized. Therefore, once the dc capacitors are charged, the dc link voltage will remain constant if no power is drawn from the capacitors. This means that the converter losses must be supplied by the grid. The angle δ in (1) should be chosen such that the sum total of the power required by the load and converter losses should flow from the source to the PCC. This can only be achieved if the dc capacitor voltage is held constant. From this logic, the following proportional plus integral (PI) controller is used to control the dc voltage.

$$\delta = K_{P\delta}\left(V_{dc}^{*} - \langle V_{dc}(t)\rangle\right) + K_{I\delta}\int\left(V_{dc}^{*} - \langle V_{dc}(t)\rangle\right)dt \qquad (2)$$

3. Operation of DC Microgrid

The DGs in the DCMG are controlled by droop equations, given by

$$\begin{aligned} V_1 &= V_{ref} - n_1 P_1 \\ V_2 &= V_{ref} - n_2 P_2 \end{aligned} \qquad (3)$$

where n_1 and n_2 are the droop gains. It can be shown that under the assumptions $n_1 >> R_1$ and $n_2 >> R_2$, the power sharing will be governed by the droop gains, i.e.,

$$\frac{P_1}{P_2} \approx \frac{n_2}{n_1} \qquad (4)$$

It is to be noted that if the droop gains are much higher than the line resistances, the power sharing is more accurate. However they also cause voltage drop in the line.

3.1. Droop Gain Selection

The DCMG is supplied by DGs that have their maximum capacity. The droop gains are chosen such that at their maximum capacity the voltage drop is limited to $\Delta V_{max} = V_{ref} - V_{min}$. Let us assume that an arbitrary DG supplies a maximum power of P_{max}. Then from (1), we get

$$\Delta V_{\max} = V_{ref} - V_{\min} = n \times P_{\max} \qquad (5)$$

Therefore the droop gain is calculated as

$$n = \frac{\Delta V_{\max}}{P_{\max}} \qquad (6)$$

Knowing the power ratings of the DGs, their droop gains can be computed from (4).

3.2. DC-DC Converter Linearized Model

The schematic diagram of a boost converter is shown in Fig. 2 (a). The switch *S* is switched on and off periodically as shown in Fig. 2 (b). If the switching frequency is *f*, then the time period between two successive switching is $T = 1/f$. If the duty ratio is denoted by *D*, the time duration $t_1 - t_0$ is equal to DT and the time duration $t_2 - t_1$ is equal to $(1 - D) \times T$.

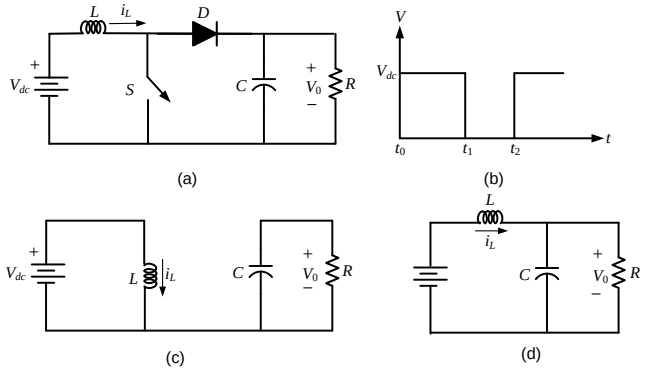

Fig. 2. *(a) Schematic diagram of a boost converter; (b) its switching sequence; equivalent circuit when the switch (c) is closed and (d) is open.*

The equivalent circuit for the switch open and closed states are shown in Fig. 2 (c) and (d) respectively. Defining a state vector as $x = [V_0 \;\; i_L]^T$, the state space description of the system can be written as

$$\dot{x} = \begin{cases} A_1 x + B_1 V_{dc} & \text{for } t_0 \le t < t_1 \\ A_2 x + B_2 V_{dc} & \text{for } t_1 \le t < t_2 \end{cases} \qquad (7)$$

where the system matrices are derived from the equivalent circuits of Fig. 2 (c) and (d).

We define t_0 as the sampling instant k and t_2 as the instant $k + 1$. Then linearizing the system around the nominal values of x_0 and D_0, we get the following linearized description of the state space system [9, 10]

$$\tilde{x}(k+1) = A\tilde{x}(k) + G\tilde{D}(k) \qquad (8)$$

where over-tilde defines the perturbed variables. Since the output is the capacitor voltage, the output equation is given by

$$\tilde{y}(k) = \begin{bmatrix} 1 & 0 \end{bmatrix}\tilde{x}(k) \qquad (9)$$

Note that a dc-dc converter may be of the type buck, boost or buck-boost. However all of them will have a linearized state space description of the form given by (8) and (9). All the converters in the dc microgrid are controlled in a state feedback with integral control as discussed in the next section.

4. Dual Active Bridge Modelling and Control

The schematic diagram of a dual active bridge bi-directional dc-dc converter is shown in Fig. 3 (a). It contains two H-bridges that are connected together through a high frequency transformer. Here L is the leakage inductance of the transformer and any added inductance, while R represents the losses.

There are different control strategies of DAB such as single phase shift (SPS) control, extended phase shift control, dual phase shift control and triple phase shift control [11]. In the SPS control, the cross connected switches of the H-bridge are provided same rectangular pulse and the other two switches are provided a complementary phase shifted rectangular pulse. In the other H-bridge the switching pulses are phase shifted from the first one. By controlling the phase shift, the output voltage and the power flow in the desired direction can be achieved. In this research work, the SPS control method is selected. the SPS control, the cross connected switches of the H-bridge are provided same rectangular pulse and the other two switches

Since the DAB contains two H-bridge converters, this has four possible switching states, given by

$$v_p = \begin{cases} V_{dc} & \text{when } S_1 \text{ is ON and } S_2 \text{ is OFF} \\ -V_{dc} & \text{when } S_2 \text{ is ON and } S_1 \text{ is OFF} \end{cases}$$
$$v_s = \begin{cases} V_0 & \text{when } S_3 \text{ is ON and } S_4 \text{ is OFF} \\ -V_0 & \text{when } S_4 \text{ is ON and } S_3 \text{ is OFF} \end{cases} \quad (10)$$

It is assumed that both the H-bridges are operated at 50% duty ratio. However their switching is shifted by an instant ϕ as shown in Fig. 3 (b). The phase shift ϕ is the control variable.

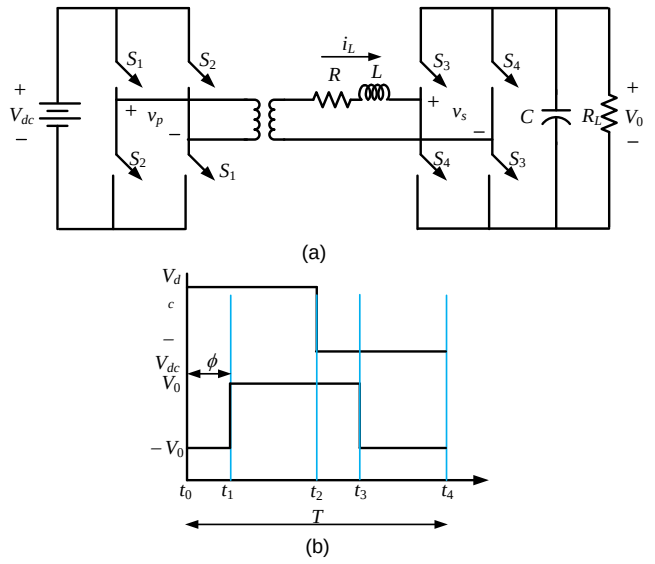

Fig. 3. *(a) Schematic diagram of a DAB and (b) its switching states.*

A sequence of 4 state space equations can be written to represent the behaviour of the DAB over one switching cycle:

$$\dot{x} = \begin{cases} A_1 x + B_1 V_{dc} & \text{for } t_0 \le t < t_1 \\ A_2 x + B_2 V_{dc} & \text{for } t_1 \le t < t_2 \\ A_3 x + B_3 V_{dc} & \text{for } t_2 \le t < t_3 \\ A_4 x + B_4 V_{dc} & \text{for } t_3 \le t < t_4 \end{cases} \quad (11)$$

where

$$A_1 = A_4 = \begin{bmatrix} -1/R_L C & -1/C \\ 1/L & -R/L \end{bmatrix}, A_2 = A_3 = \begin{bmatrix} -1/R_L C & 1/C \\ -1/L & -R/L \end{bmatrix}$$
$$B_1 = B_2 = \begin{bmatrix} 0 \\ 1/L \end{bmatrix}, B_3 = B_4 = \begin{bmatrix} 0 \\ -1/L \end{bmatrix}$$

We note from Fig. 3 (b) that $t_1 - t_0 = \phi$, $t_2 - t_1 = T/2 - \phi$, $t_3 - t_2 = \phi$ and $t_4 - t_3 = T/2 - \phi$. Also since all the A matrices are non-singular, the solutions of the four state equations are given by

$$x(t_1) = e^{A_1\phi} x(t_0) - A_1^{-1}\left[I - e^{A_1\phi}\right] B_1 V_{dc} \quad (12)$$
$$x(t_2) = e^{A_2(T/2-\phi)} x(t_1) - A_2^{-1}\left[I - e^{A_2(T/2-\phi)}\right] B_2 V_{dc} \quad (13)$$
$$x(t_3) = e^{A_3\phi} x(t_2) - A_3^{-1}\left[I - e^{A_3\phi}\right] B_3 V_{dc} \quad (14)$$
$$x(t_4) = e^{A_4(T/2-\phi)} x(t_3) - A_4^{-1}\left[I - e^{A_4(T/2-\phi)}\right] B_4 V_{dc} \quad (15)$$

Substituting (12) in (13), then the resulting equation in (14) and finally to (15), we get a relationship between $x(t_4)$ and $x(t_0)$ as

$$x(t_4) = F x(t_0) + G V_{dc} \quad (16)$$

Defining t_0 as the sampling instant k and t_4 as the sampling instant $k + 1$, and linearizing (18), we get

$$\tilde{x}(k+1) = A\tilde{x}(k) + B\tilde{\phi}(k)$$
$$\tilde{y}(k) = \begin{bmatrix} 1 & 0 \end{bmatrix}\tilde{x}(k) \quad (17)$$

where

$$A = \frac{\partial F}{\partial x}, \quad B = \frac{\partial F}{\partial \phi} + \frac{\partial G}{\partial \phi}$$

4.1. State Feedback Control

A state feedback with integral control law is designed for the system given in (17). For this, discrete-time integral

controller of the form given in (18) is used where y_{ref} is the reference voltage.

$$\begin{aligned} e(k) &= \tilde{y}(k) - \tilde{y}_{ref}(k) \\ z(k) &= z(k-1) + K_I e(k) \end{aligned} \tag{18}$$

Substituting (18) in (17), we get

$$z(k+1) = z(k) + K_I C_1 \tilde{x}(k+1) - K_I \tilde{y}_{ref}(k+1) \tag{19}$$

An extended state vector is now defined as

$$x_e(k) = \begin{bmatrix} \tilde{x}(k) \\ z(k) \end{bmatrix}$$

Then from (17) and (19), the extended state space description of the system can be written as

$$x_e(k+1) = \begin{bmatrix} A & 0 \\ K_I C_1 & 1 \end{bmatrix} x_e(k) + \begin{bmatrix} B \\ 0 \end{bmatrix} \tilde{\phi}(k) - \begin{bmatrix} 0 \\ K_I \end{bmatrix} \tilde{y}_{ref}(k) \tag{20}$$

A state feedback controller is then designed that is of the form

$$\tilde{\phi}(k) = -K x_e(k) \tag{21}$$

The gain matrices are now chosen using discrete-time linear quadratic regulator, which will force the output error $e(k)$ to zero asymptotically.

4.2. Steady State Calculation

If the converter is assumed to be lossless, the power transfer relationship is given by [12, 13]

$$P_1 = P_2 = \frac{V_{dc} V_0 \phi(\pi - \phi)}{2\pi^2 fL} \tag{22}$$

Therefore the power transfer is zero either when $\phi = 0$ or when $\phi = \pi$ and the maximum power is transferred when $\phi = \pi/2$. For the state feedback control of (21), a linearized model of the system is required. From (22), it can be seen for constant V_{dc}, P_2 and ϕ, the output voltage V_0 will change with the output resistance. The first step in the linearization process is to decide a nominal value of the output power P_{20}. Therefore by choosing a nominal output voltage V_{00}, the load resistance can then be given by $R_L = (V_0)^2/P_{20}$. Now (22) can be rewritten as

$$\phi^2 - \pi\phi + \frac{2\pi^2 fL}{V_{dc} V_{00}} P_{20} = 0 \tag{23}$$

Solving the quadratic equation and choosing the lesser of the two values, the nominal value of the phase shift ϕ_0 is obtained. Therefore, with these values, the steady state values of the state vector is computed from (16) as

$$x_{ss} = (I - F)^{-1} G V_{dc} \tag{24}$$

These are now used for linearized model and control derivation.

4.3. Power Flow Control

Comparing Fig. 3 (a) with Fig. 1 (a), it is obvious that input voltage V_{dc} is V_{dc1} and the output voltage V_0 is V_{dc2}. While the former is controlled by the interlinking converter (Section 2), the reference for latter is determined by the desired link power transfer. Let us denote the desired link power by P_{link}^*. Then the reference voltage for the DAB is obtained though the following proportional plus integral (PI) controller

$$\begin{aligned} e_l &= P_{link}^* - P_{link} \\ V_{dc2,ref} &= V_{ref} - K_{Pl} e_l - K_{Il} \int e_l dt \end{aligned} \tag{25}$$

5. Simulation Results

Simulation studies are carried out in PSCAD, with the system data given in Table 1. The control parameters for the DAB, three dc-dc converters and the VSC are calculated in MATLAB and then are used to run simulations in PSCAD. Three case studies are performed. These are discussed below.

Case 1: Nominal Operation

In this case, it is assumed that no power flows through the DAB and the utility side and the DCMG perform in isolated fashion. The nominal phase shift in the DAB is calculated as per equation 23, for an input voltage of 15 kV, the output voltage will be 500 V. The total load in the DCMG is 78.5 kW and the power generated by the two DGs are 48.7 kW and 24.6 kW. For this power level, the voltages V_1 and V_2 will be roughly around 475 V. Also the power supplied by the utility to supply its local loads and the converter losses is 565 kW.

With the system remaining in the steady state, the DCMG load is changed to 148.5 kW at 0.3 s. The results are shown in Fig. 4. Fig. 4(a) shows the performance of the utility and IC, where it can be seen that, barring a transient during the load change, the utility power, dc capacitor voltage V_{dc1}

and voltage angle δ maintain their pre-load change values. The performance of the DCMG is depicted in Fig. 4(b). It can be seen that the power supplied by the DGs rises to 101 kW and 51 kW to cater to the load change. The voltages V_1 and V_2 drop to around 449.5 V in sympathy with the load change.

Table 1: System parameters

Quantities	Values
AC Side	
AC source voltage	11 kV (L-L)
System frequency	50 Hz
AC feeder impedance	Inductance: 38.6 mH and resistance: 1.21 Ω
Filter parameters	L_f = 33 mH, C_f = 50 μF
Interlinking Converter	
DC Capacitor (C_{dc1})	5000 μF
Voltage Magnitude (V_m)	9 kV (peak)
Carrier waveform	15 kHz
Sampling frequency	30 kHz
DC voltage reference (V_{dc}^*)	15 kV
PI controller	$K_{P\delta}$ = – 0.1, $K_{I\delta}$ = – 0.5
DAB	
Transformer	2.5 kV/2.5 kV
Inductance	L = 0.4 mH
Switching frequency	10 kHz
PI controller	K_{Pl} = 2, K_{Il} = 100
DC Capacitor (C_{dc2})	5000 μF
DCMG	
Voltage reference (V_{ref})	500 V
Maximum voltage drop (ΔV)	100 V
DG rating	DG-1: 200 kW, DG-2: 100 kW
Droop gains	n_1 = 0.5, n_2 = 1.0
Line resistances	R_1 = 0.01 Ω, R_2 = 0.06 Ω, R_3 = 0.001 Ω

The performance of the DAB is shown in Fig. 4(c). It can be seen that the phase shift and hence the power flow through the link (P_{link}) remain zero as no power between the ac and dc systems are desired. This figure also shows the dc voltage V_{dc2} and its reference. It can be seen the voltage tracking by the DAB is perfect. Also these voltages have drop after the load change to maintain zero power flow since V_1 and V_2 have dropped.

Case 2: Power flow from DCMG to AC Grid

At the beginning of this case, it is assumed that no power flows through the DAB. The total load in the DCMG is 160 kW and the power generated by the two DGs are 108 kW and 54 kW. The voltages V_1 and V_2 are roughly around 446 V. The power supplied by the utility s is 565 kW. With the system operating in the steady state, the power reference through the link is changed to 50 kW at 0.3 s, such that this amount of power flows to the utility grid. The results are shown in Fig. 5.

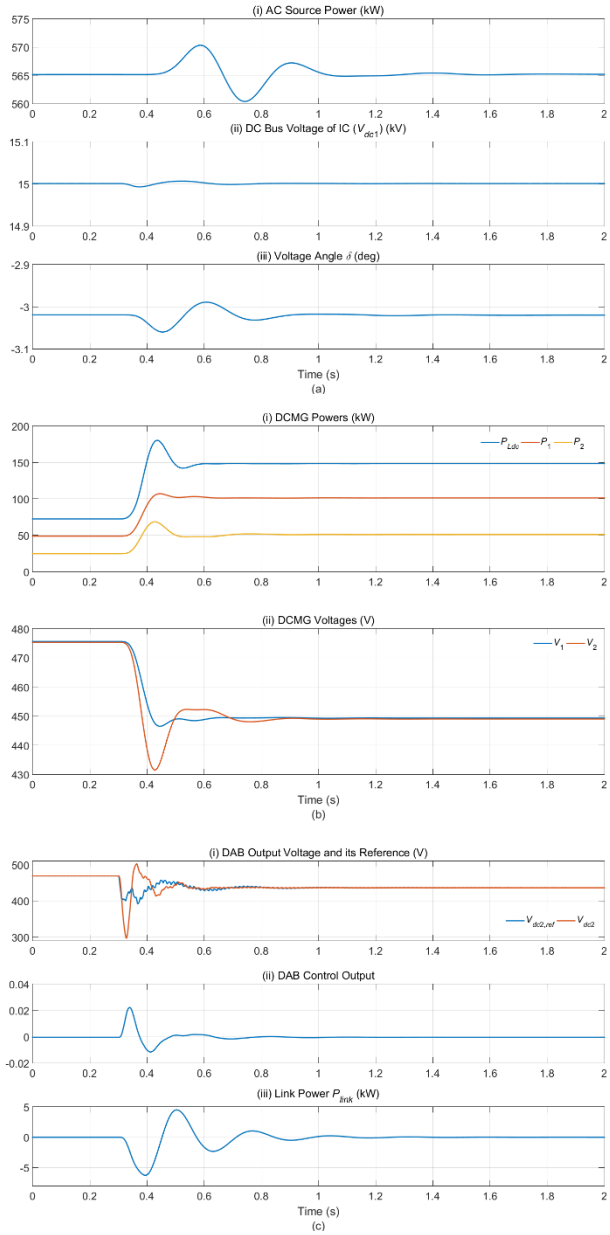

Fig. 4(a). *Performance of utility and IC for Case 1: (i) source power, (ii) dc link voltage and (iii) voltage angle.* ***(b)*** *Performance of DCMG for Case 1: (i) power flow and (ii) voltages.* ***(c)*** *Performance of DAB for Case 1: (i) voltage V_{dc2} and its reference, (ii) phase shift and (iii) power flow through the link.*

Fig. 5(a-i) shows that the power supplied by the utility reduces to 516 kW as expected. The capacitor voltage V_{dc1} is maintained at 15 kV, as shown in Fig. 5(a-ii). The voltage angle however becomes smaller since the utility supplies less amount of power. From Fig. 5 (b-i), it can be seen that the power consumed by the dc load remains constant at 160 kW. However due to the extra amount of power supplied to the ac

side, the DGs now supply 145 kW and 72 kW. The link power settles to 50 kW. Due to the increase in the power supply by the DCMG, the voltages drop to 427 V.

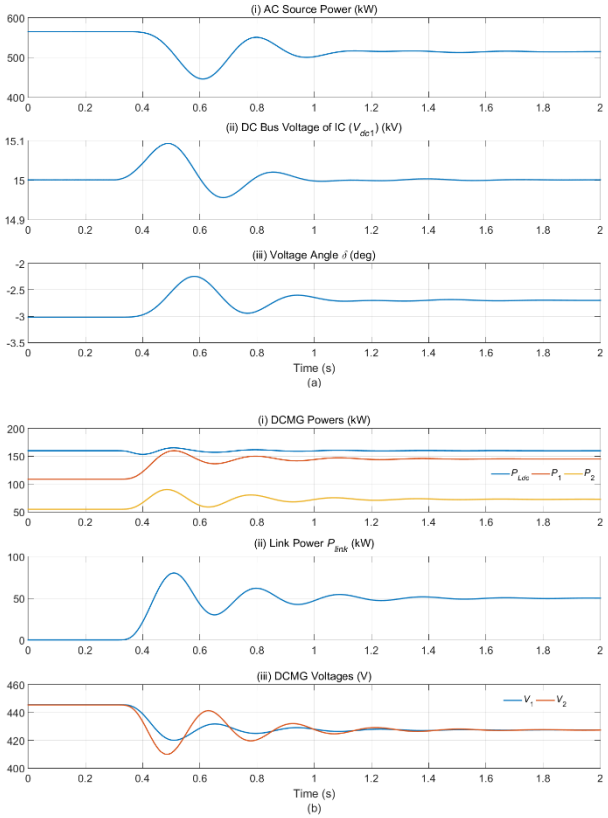

Fig. 5 (a). *Performance of utility and IC for Case 2: (i) source power, (ii) dc link voltage and (iii) voltage angle.* ***(b).*** *Performance of DCMG for Case 2: (i) power flow, (ii) link power and (iii) voltages.*

Case 3: Power flow from AC Grid to DCMG

In this case, it is assumed that the utility grid starts supply 100 kW of power to the DCMG at 0.3 s when the systems are in the steady state and operating in isolated fashion. The total load in the DCMG is 202 kW and the power generated by the two DGs are 140 kW and 70 kW. The voltages V_1 and V_2 are roughly around 430 V. The power supplied by the utility s is 565 kW. The results are shown in Fig. 6.

Fig. 6 (a) shows that the power supplied by the utility increases to 665 kW. The capacitor voltage V_{dc1} is maintained at 15 kV and the voltage angle decreases to accommodate increased power flow from the utility. The results for the DCMG side are shown in Fig. 6(b). As evident from this figure, the power consumed by the dc load remains constant, however the DGs now supply less amount of power of 70 kW and 35 kW. The link power settles is – 100 kW. Due to the decrease in the power supplied by the DGs, the voltages rise to 465 V.

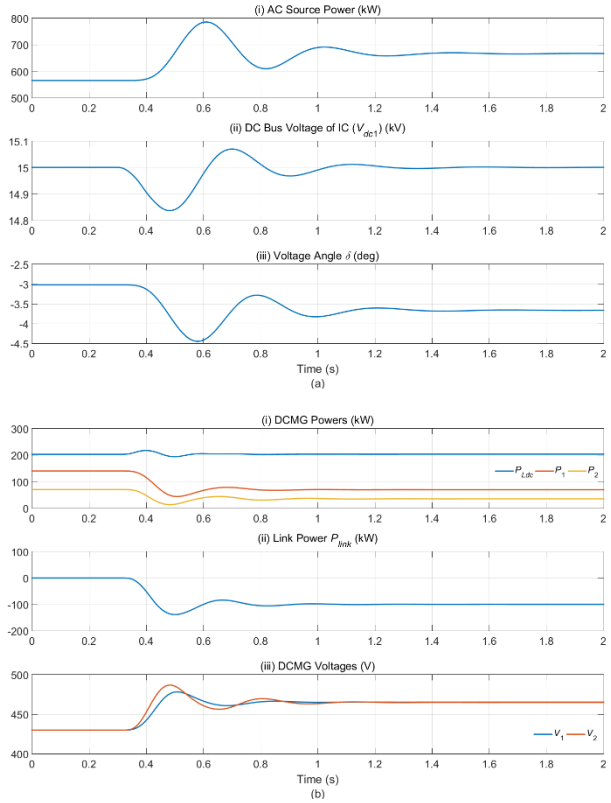

Fig. 6 (a). *Performance of utility and IC for Case 3: (i) source power, (ii) dc link voltage and (iii) voltage angle.* ***(b)*** *Performance of DCMG for Case 3: (i) power flow, (ii) link power and (iii) voltages.*

6. Experimental Results

Hardware test results of nominal operation and power flow from AC grid to DCMG are reported in this section. A scaled prototype of the DCMG with a DAB is implemented for experimental verification of the proposed control scheme. Simulation results of the same hardware prototype is also presented in this section. DSPACE-1104 is used to measure the control parameters and then to implement the proposed control scheme. The experimental system is also simulated in PSCAD. A photograph of the hardware setup is shown in Fig. 7 and the system parameters of the hardware prototype is presented in Table 2.

The hardware prototype of DAB is operated at a frequency of 2 kHz. The switching pulses of S_1, S_2, S_3 and S_4 are shown in Fig. 8. It is evident that the switches operate with 50% duty ratio. The phase shift is also evident in this figure.

During Nominal operation, DCMG is self-sufficient and hence no power needs to be supplied by the utility through the DAB. It has been assumed that the rating of the two DGs have a ratio of 2:1 and together they have a maximum rating of 0.6 p.u. The power supplied by the DGs are shown in Fig. 9-i (simulation) and Fig. 10-i (hardware) when the load is 0.6 p.u. The DG voltages and currents are also shown in these figures.

Table 2: Hardware prototype parameters

DAB	
Inductance	L = 2.2 mH
Switching frequency	2 kHz
DC Capacitor (C_{dc2})	1100 µF
DCMG	
Voltage reference (V_{ref})	15 V
Maximum voltage drop (ΔV)	5 V
DG rating	DG-1: 30 W, DG-2: 15 W
Droop gains	n_1 = 0.5, n_2 = 1.0
Line resistances	R_1 = 1.1 Ω, R_2 = 1.3 Ω, R_3 = 1.2 Ω

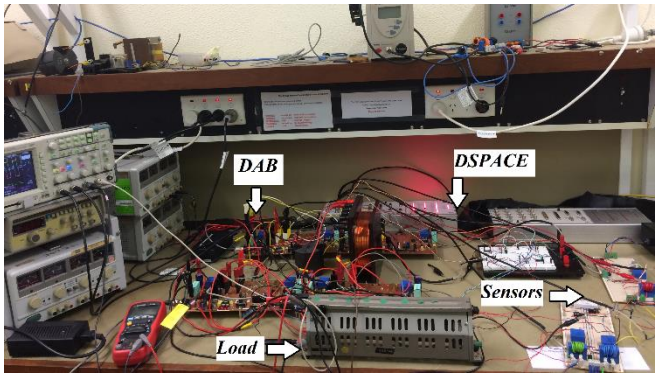

Fig. 7. *Hardware prototype of the system*

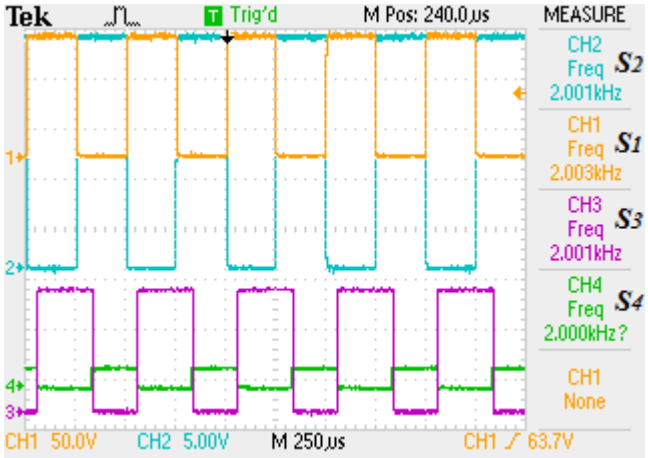

Fig. 8. *Firing pulses of the DAB switches.*

Fig 9-ii and 10-ii show the DAB output voltage, current and power when the utility supplies power to the DCMG. When the load is load is increased to 0.77 p.u., the additional power is supplied to the load through DAB. When the load is increased to 0.8 p.u, power through the DAB becomes 0.2 p.u. The simulation results and the hardware results are shown in Fig 9-iii and Fig. 10-iii.For this case, the flow from the DAB increases and its output voltage drops. It can be noticed from this study that the hardware results have some ripple.

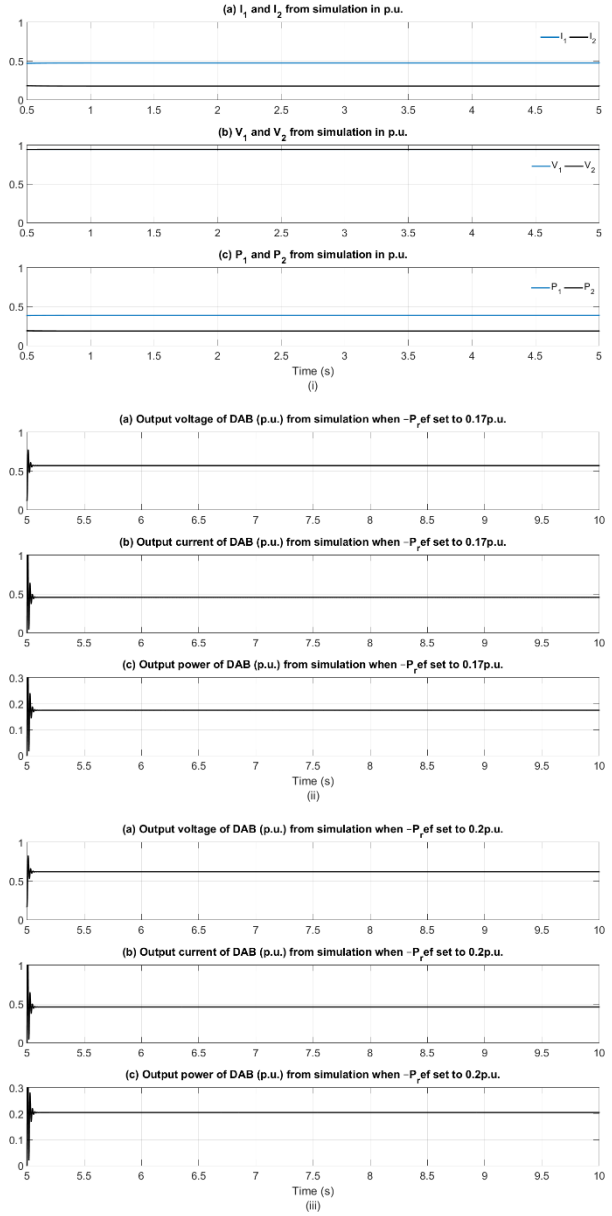

Fig. 9. *Simulation results of the DCMG at Nominal operation (i) and performance of the DAB at -P_{ref} set to 0.17 p.u.(ii) and 0.2 p.u. (iii)*

7. Conclusion

In this paper, the operation and control of a utility connected dc microgrid are discussed. The dc microgrid is connected to the utility through a DAB and an interlinking converter. The DAB facilitates a bidirectional power flow, which is advantageous since a specified amount of power can be drawn from the utility thereby obviating the need of battery backup. Also during peak power generation in the dc microgrid (may be through renewable sources), the excess power can be sold to the utility.

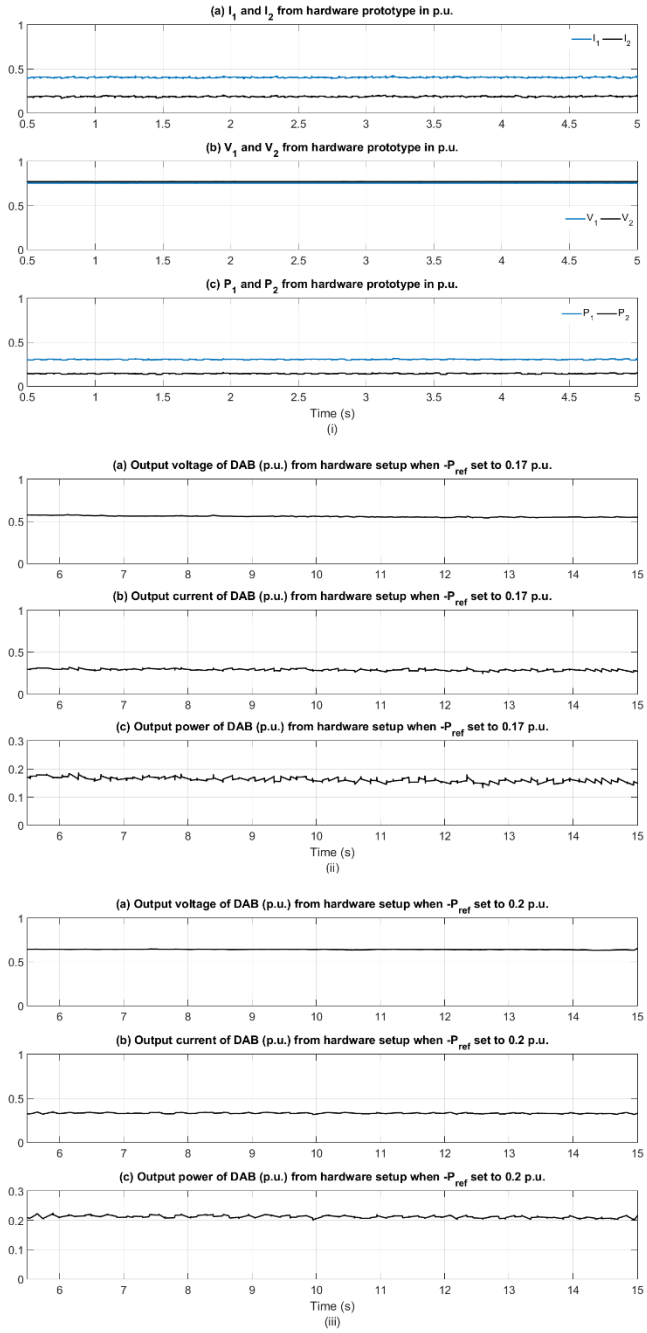

Fig. 10. *Hardware result of the DCMG at Nominal operation (i) and performance of the DAB at -P_{ref} set to 0.17 p.u.(ii) and 0.2 p.u. (iii)*

For the bidirectional power flow control, two separate PI controllers are designed and tuned. A small signal model of the DAB has been derived based on state transition equation, where the continuity of the state variables during the switching operation has been retained. The small signal model has the phase shift as the input variable and this is regulated around it steady state value to facilitate power flow. For this model, the steady state value is obtained for any particular value of output power. A DLQR with integral controller has been designed and, as the results show, this controller is fairly robust. The veracity of the scheme is verified through both simulation and experimental results.

8. Acknowledgement

The authors thank the Australian Research Council (ARC) for the financial support for this project through the ARC Linkage Grant LP140100586.

9. References

[1] K. Shenai and K. Shah, "Smart DC Micro-grid for Efficient Utilization of Distributed Renewable Energy," IEEE EnergyTech, Cleveland, 2011.

[2] X. Liu, P. Wang, and P. C. Loh, "A Hybrid AC/DC Microgrid and Its Coordination Control," IEEE Transactions on Smart Grid, Vol. 2, No. 2, pp. 278-286, 2011.

[3] P. C. Loh, D. Li, Y. K. Chai, and F. Blaabjerg, "Autonomous Operation of Hybrid microgrid with AC and DC Subgrids," IEEE Transactions on Power Electronics, Vol. 28, No. 5, pp. 2214-2223, 2013.

[4] A. Navarro-Rodriguez, P. Garcıa et al, "Adaptive Active Power Sharing Techniques for DC and AC Voltage Control in a Hybrid DC/AC Microgrid," IEEE ECCE, Cincinnati, OH, USA 2017.

[5] G. Qi, A. Chen and J. Chen, "Improved Control Strategy of Interlinking Converters with Synchronous Generator Characteristics in Islanded Hybrid AC/DC Microgrid," CPSS Transactions on Power electronics and Applications, Vol. 2, No. 2, pp. 149-158, 2017.

[6] Y. Xia, Y. Peng, et al, "Distributed coordination control for multiple bidirectional power converters in a hybrid ac/dc microgrid," IEEE Transactions on Power Electronics, Vol. 32, No. 6, pp 4949-4959, 2017.

[7] A. J. Datta, A. Ghosh and S. Rajakaruna, "Power Sharing in a Hybrid Microgrid with Bidirectional Switch," IEEE PES General Meeting, Chicago, 2017.

[8] D. Kumar, F. Zare and A. Ghosh, "DC Microgrid Technology: System Architectures, AC Grid Interfaces, Grounding Schemes, Power Quality, Communication Networks, Applications and Standardizations Aspects

[9] A. Ghosh and G. Ledwich, "Modelling and Control of Switch-mode DC-DC Converters using State Transition Matrices," International journal of electronics, Vol. 79, No. 1, pp. 113-127, 1995.

[10] A. J. Datta, A. Ghosh and S. Rajakaruna, "Power Sharing and Management in a Utility Connected DC Microgrid," Australasian Universities Power Engineering Conference (AUPEC), Melbourne, 2017.

[11] B. Zhao, Q. Song, et al, "Overview of Dual Active Bridge Isolated Bidirectional Dc-Dc Converter for High-Frequency-Link-Power-Conversion System," IEEE Transactions on Power Electronics, Vol. 29, No. 8, pp 4091-4106, 2014.

[12] R.W. A. A. De Doncker, D. M. Divan and M. H. Kheraluwala, "A Three-phase Soft-Switched High-Power-Density DC/DC Converter for High-Power

Applications," IEEE Trans. Ind. Appl., vol. 27, no. 1, pp. 63–73, 1991.

[13] F. Krismer and J. W. Kolar, "Accurate Small-Signal Model for the Digital Control of an Automotive Bidirectional Dual Active Bridge," IEEE Transactions on Power Electronics, Vol. 24, No. 12, pp 2756-2768, 2009.